Endocardial HDAC3 is required for myocardial trabeculation

Jihyun Jang[1,2], Mette Bentsen[3], Ye Jun Kim[4], Erick Kim[4], Vidu Garg[1,2], Chen-Leng Cai[5], Mario Looso[3], Deqiang Li[1, 2]

[1]Center for Cardiovascular Research, Abigail Wexner Research Institute, Nationwide Children's Hospital, Columbus, OH 43215, USA

[2]Department of Pediatrics, The Ohio State University College of Medicine, Columbus, OH 43215, USA

[3]Bioinformatics Core Unit (BCU), Max Planck Institute for Heart and Lung Research, 61231, Bad Nauheim, Germany

[4]Department of Surgery, University of Maryland School of Medicine, Baltimore, MD 21201, USA

[5]Department of Pediatrics, Herman Wells Center for Pediatric Research, Indiana University School of Medicine, Indianapolis, IN 46201, USA

Address correspondence to:

Deqiang Li, MD&PhD

575 Children's Drive, Room WB4329,

Columbus, OH 43215, USA

Phone: 614-355-5826

Email: Deqiang.Li@nationwidechildrens.org

Abstract

Failure of proper ventricular trabeculation is often associated with congenital heart disease (CHD). Support from endocardial cells, including the secretion of extracellular matrix (ECM) and growth factors is critical for trabeculation. However, it is poorly understood how the secretion of ECM and growth factors is initiated and regulated by endocardial cells.

We found that genetic knockout (KO) of histone deacetylase 3 (*Hdac3*) in the endocardium in mice resulted in early embryo lethality and ventricular hypotrabeculation. Single cell RNA sequencing identified significant downregulation of ECM components in *Hdac3* KO endocardial cells. Secretome from cultured *Hdac3* KO mouse cardiac endothelial cells lacked transforming growth factor ß3 (TGFß3) and showed significantly reduced capacity in stimulating cultured cardiomyocyte proliferation, which was remarkably rescued by TGFß3 supplementation. Mechanistically, we identified that HDAC3 induced *Tgfß3* expression through repressing microRNA (miR)-129-5p.

Our findings provide novel insights into the pathogenesis of CHD and conceptual strategies to promote myocardial regeneration.

Introduction

Congenital heart disease (CHD) is the most common congenital disorder, and the leading cause of mortality from birth defects[1]. Defective myocardial growth is either the primary manifestation or associated with many forms of CHD[2, 3]. In the early primitive heart (mouse embryonic day 8-10), inner cardiac endothelial cells (CECs), also called endocardial cells, and outer cardiomyocytes (CMs), which are separated by extracellular matrix (ECM), co-contribute to early myocardial trabeculation (i.e., formation of myocardial meshwork extending to cardiac chamber)[4, 5, 6]. CECs juxtapose myocardial trabeculae and lead myocardial trabeculation by secretion of growth factors such as Neuregulin 1 (NRG1) and transforming growth factor ß (TGFß)[2, 3, 5]. Meanwhile, CECs support trabeculation by secreting ECM (e.g., various collagens, versican) that facilitate the travelling of CEC secreted growth factors to trabecular myocardium and support trabecular CM proliferation[4, 7]. Surprisingly, disruption of ECM components alone (e.g., hyaluronan synthase-2, versican) prevents the proper formation of trabeculae in mice[8, 9]. Although CECs play such important roles during ventricular trabeculation, it remains poorly understood how these ECM proteins and growth factors are regulated in the developing CECs.

TGFß signaling pathway is involved in many fundamental cellular processes in both adults and developing embryos including cell proliferation, differentiation, migration, and apoptosis[10, 11]. The TGFß superfamily includes many different ligands (e.g., Bone morphogenetic proteins, Growth and differentiation factors, Activin, Nodal, TGFß). These ligands bind to their specific type II receptors, which triggers phosphorylation of type I receptor, eventually leads to phosphor-Smad2/3 localized to the nucleus and drives a

64 variety of downstream target gene expression, which is the canonical TGFß signaling
65 pathway[12]. In addition, the binding of ligands to receptors can also directly activate
66 multiple non-Smad mediated intracellular signaling pathways such as MAP kinase
67 pathways and phosphatidylinositol-3-kinase/AKT pathways[13, 14]. These non-Smad
68 (noncanonical) TGFß signaling pathways are equally critical for driving some specific
69 cellular processes (e.g., cell proliferation, cell survival, endothelial/epithelial
70 mesenchymal transition)[13, 14]. During cardiovascular development, unsurprisingly, TGFß
71 signaling is implicated in most morphological events including cardiac lineage
72 specification, cardiac looping, valvogenesis, and cardiomyogenesis[15]. The TGFß family
73 includes TGFß1, TGFß2, and TGFß3. Although TGFß1, TGFß2 and TGFß3 are
74 abundantly expressed in the developing endocardium and epicardium, it appears that
75 they do not perform redundant functions: individual knockout results in different
76 phenotypes[15]. For instance, global knockout of either *Tgfß2* or *Tgfß3* result in early
77 perinatal lethality, presenting hypoplastic hearts with thin myocardium[16, 17], suggesting
78 that they play critical roles for myocardial growth. In contrast, global knockout of *Tgfß1*
79 lead to partial embryonic lethality with survivors appearing phenotypically normal in first
80 the two weeks of life[18]. Nonetheless, it is poorly understood how the expression of TGFß
81 ligands are regulated in the early developing heart.
82 Epigenetic modulators such as histone deacetylases (HDACs) are critical for early heart
83 development as key regulators of regulating gene expresison[19, 20]. There are 18 known
84 human HDACs, which can be subdivided into four classes based on their function and
85 DNA sequence similarity. Class I HDACs include HDAC1, HDAC2, HDAC3, and HDAC8,
86 and are predominantly nuclear and ubiquitously expressed[21]. Although class I HDACs

87 have high degree of homology, global knockout of each causes early embryonic lethality[19],
88 suggesting distinct roles during early heart development. Global deletion of *Hdac3* leads
89 to early embryonic lethality at gastrulation[22]. In the developing heart, lack of *Hdac3* in
90 cardiac progenitors disrupts secondary heart field development[23], lymphovenous valve
91 morphogenesis[24], and CM lineage specification[25]. Recently, we reported that HDAC3 in
92 the developing epicardium plays a critical role in supporting compact myocardial wall
93 expansion[26]. It is unclear whether or how HDAC3 in the developing endocardium impacts
94 myocardial trabeculation.
95 In the current study, we investigated the role of HDAC3 in the developing endocardium
96 during early heart development.

97 **Results**

98 **Endothelial/Endocardial cell specific deletion of *Hdac3* results in embryonic**
99 **lethality and hypotrabeculation.**

100 To study the role of HDAC3 in the cardiac endothelium during early heart development,
101 *Hdac3* was specifically deleted in the endothelial cells using *Tie2-Cre*[27], while its
102 expression in other cells including CMs remains intact (Supplemental Figure 1). Note:
103 since *Tie2-Cre* is transiently expressed in oocytes[28], the mating scheme was always
104 *Hdac3*$^{f/+}$*; Tie2-Cre/+* (♂) and *Hdac3*$^{f/f}$ (♀). By recovering the progenies at a series of
105 embryonic and postnatal stages, we identified that *Hdac3* KO in the developing
106 endothelium resulted in early embryonic lethality starting at E12.5 (Supplemental Table
107 1). To investigate the potential cause of early embryonic lethality, we performed
108 histological analyses. Interestingly, in Tie2 endothelial *Hdac3* KO embryos (*Hdac3*^{tko}),
109 there was no noticeable phenotype in the various endothelial cell derived tissue where
110 the *Tie2*-lineage contributes, such as endocardium (Figure 1, Supplemental Figure 2) and
111 blood vessels (Supplemental Figure 3), given that *Tie2-Cre* is active in all endothelial cells
112 in the body[29]. In contrast, there were myocardial defects in *Hdac3*^{tko} embryos starting at
113 E11.5: *Hdac3*^{tko} trabeculae appeared to be significantly sparser and shorter as compared
114 to the thick and long webbing like trabecular network in littermate control hearts
115 (Supplemental Figure 2). This cardiac phenotype in *Hdac3*^{tko} mice was more prominent
116 at E12.5 (Figure 1A). The compact layer was also significantly thinner in *Hdac3*^{tko} hearts.
117 To further validate the myocardial trabecular phenotype in endothelial *Hdac3* deleted
118 hearts, we specifically deleted *Hdac3* in the endocardium using *Nfatc1*$^{Cre/+}$, endocardial
119 specific Cre[30], which also resulted in embryonic lethality (Supplemental Table 2).

120 *Hdac3*^{nko} (*Hdac3*$^{f/f}$*; Nfatc1*$^{Cre/+}$) hearts presented a similar cardiac phenotype, albeit at a
121 later stage (E14.5): smaller and sparser trabeculae, thinner compact wall (Supplemental
122 Figure 4). This is consistent with the achievement of late deletion of *Hdac3* in the
123 endocardium by *Nfatc1*$^{Cre/+}$ (Supplemental Figure 4). Nonetheless, these results confirm
124 that the cardiac phenotypes resulting from *Tie2* endothelial *Hdac3* deletion are primarily
125 from the endocardium, and not secondary to another endothelium (e.g., vascular).
126 *Hdac3*^{tko} embryos were used for all subsequent mechanistic studies.
127
128 **Endothelial *Hdac3* knockout hearts display decreased trabecular CM proliferation.**
129 Next, we investigated whether altered cell proliferation and/or apoptosis contribute to the
130 hypotrabeculation phenotypes in *Hdac3*^{tko} hearts. At E11.5, the percentage of either p-
131 H3+ or BrdU+ CMs is significantly lower in *Hdac3*^{tko} trabecular and compact myocardium
132 as compared to littermate control hearts (Figure 1B). This finding is consistent with the
133 hypoplastic cardiac phenotypes seen in *Hdac3*^{tko} hearts (Figure 1A). In contrast, there
134 was no significant difference in cell apoptosis between *Hdac3*^{tko} hearts and littermate
135 control hearts (Supplemental Figure 5). Decreased CM proliferation of *Hdac3*^{tko} hearts
136 may result from disrupted communication from the endocardium to the trabecular
137 myocardium. We performed single cell RNA-sequencing (scRNA-seq) on E11.5 *Hdac3*^{tko}
138 hearts and littermate control hearts (Figure 2A). We obtained high-quality scRNA-seq
139 profiles for 23,468 and 25,547 cells from 4 *Hdac3*^{tko} (*Hdac3*$^{f/f}$*; Tie2-Cre/+; R26*$^{eYFP/+}$) and
140 4 control (3 of *Hdac3*$^{f/+}$*; Tie2-Cre/+; R26*$^{eYFP/+}$ and 1 of *Hdac3*$^{f/+}$*; Tie2-Cre/+*) heart single
141 cell suspensions, respectively. Unsupervised clustering successfully separated 6 distinct
142 clusters including endocardial cells and CMs in these samples (Figure 2B and

143 Supplemental Figure 6). Referring to a recent transcriptome profiling methodology for
144 clustering embryonic CMs[31], we re-clustered CMs into “trabecular” and “compact” clusters
145 based on the overall scores after applying a few known trabecular and compact markers
146 (Trabecular: *Bmp10*, *Nppa* and *Thbs4*; Compact: *Hey2*, *Mycn* and *Tnnt1*) (Supplemental
147 Figure 7A and Figure 2C). Among them, *Bmp10*+ CMs nicely represent the trabecular
148 cluster (Figure 2C), and thus we focused on this population for subsequent analyses since
149 *Hdac3*^{tko} hearts mainly display hypotrabeculation phenotypes (Figure 1). Overall, the total
150 number of *Bmp10*+ trabecular CMs were not significantly different between *Hdac3*^{tko} and
151 littermate control hearts (Supplemental Figure 7B). Note: 10,000 cells/sample was
152 sequenced. Next, we performed differential gene expression (DGE) analyses on *Hdac3*^{tko}
153 and littermate control trabecular clusters. We found that the expression of eukaryotic
154 translation elongation factor 1 alpha 2 (*Eef1a2*) and early growth response 1 (*Egr1*) are
155 significantly down regulated in *Hdac3*^{tko} trabeculae as compared to control trabeculae
156 (Figure 2D). *Eef1a2* and *Egr1* are known to be critical for cell growth[32, 33, 34]. These
157 findings are consistent with reduced proliferation index seen in *Hdac3*^{tko} hearts (Figure
158 1B), suggesting myocardial growth retardation account for the hypotrabeculation
159 phenotypes in *Hdac3*^{tko} hearts.
160

161 **Endothelial HDAC3 induces ECM gene expression.**

162 Among all scRNA-seq samples, 7 of them carried *R26*$^{eYFP/+}$ reporters (3 CTL and 4
163 *Hdac3*^{tko}). This enabled us to perform a lineage specific analysis. In the single cell
164 suspension, 8.6% cells in CTL hearts and 11.2% cells in *Hdac3*^{tko} hearts were YFP+
165 (Supplemental Figure 8A). As expected, the expression of *Hdac3* in YFP+ populations in

166 *Hdac3*^{tko} hearts was significantly decreased compared to YFP+ populations in CTL hearts
167 (Supplemental Figure 8B). During early heart development, endothelial progenitors can
168 also give rise to mesenchymal cells through endothelial to mesenchymal transition[6, 35].
169 As expected, YFP+ cells (*Tie2* lineage) were primarily CECs with a minority of
170 mesenchymal cells (Figure 2E). Also, as expected, *Hdac3* expression was absent in
171 *Hdac3*^{tko} YFP+ cells. Subsequent DGE analysis did not reveal significant gene expression
172 differences between *Hdac3*^{tko} and control mesenchymal cells (Figure 2E). Instead, in
173 CEC clusters, we found that the expression of genes regulating cellular component
174 organization was highly enriched in the control YFP+ CEC cluster (Figure 2F). In
175 particular, the expression of ECM associated genes, including *Col13a1, Col1a2, Tgfbi,*
176 *Timp2, Col26a1, Col3a1, Col4a5*, *Timp3*, and *P4ha3*, was significantly reduced in
177 *Hdac3*^{tko} YFP+ CEC cluster as compared to control YFP+ CEC cluster (Figure 2G).
178 *Col1a1, Col1a2, Col2a1*, and *Col3a1* and *P4ha3* DGE was further validated in *Hdac3*^{tko}
179 and control heart lysates by qRT-PCR (Figure 2H). These results suggest that cardiac
180 endothelial HDAC3 induces the expression of ECM associated genes, which are critical
181 for CM proliferation and trabeculation growth (Figure 2I).
182

183 **Cardiac endothelial HDAC3 induces *Tgfβ3* in driving CM proliferation.**

184 Trabeculation and ECM remodeling are coordinated during early heart development, and
185 both processes are regulated by growth signaling[36]. To better identify potential growth
186 signaling pathways regulated by HDAC3 in the endocardium, we used a mouse cardiac
187 endothelial cell (MCEC) line[37]. Using CRISPR-Cas9 gene editing technology and the
188 same set of gRNAs we have recently used[26], we successfully knocked out *Hdac3* in the

189 MCECs (Figure 3A). *Hdac3* KO MCECs grew slower than *Hdac3* empty vector (EV)
190 control MCECs. To determine whether the secretome from *Hdac3* KO endothelial cells is
191 competent to induce CM proliferation, we treated cultured primary embryonic CMs
192 isolated from E13.5 *Tnnt2*$^{nGFP/+38}$ hearts with supernatant from either *Hdac3* KO MCECs
193 or *Hdac3* EV MCECs, respectively. *Hdac3* KO supernatant treatment resulted in
194 significant decrease of the percentage of Ki67+ CMs and the total number of CMs, as
195 compared to *Hdac3* EV supernatant treatment (Figure 3B). These results suggest that
196 growth signals derived from CECs required to support CM proliferation may be
197 inadequate/deficient in *Hdac3* KO MCECs, and the incompetent secretome from *Hdac3*
198 KO endothelial cells may contribute to the hypotrabeculation phenotype. Indeed,
199 treatment of wildtype MCEC supernatants but not control media (DMEM/F-12 without any
200 serum or growth factor supplementation) successfully rescued the hypotrabeculation
201 phenotype in *ex vivo* cultured E11.5 *Hdac3*^{tko} hearts (Supplemental Figure 11). To
202 unbiasedly search for such growth signals, we performed bulk RNA-Seq analyses on
203 *Hdac3* KO and EV MCECs; we identified 484 downregulated and 239 upregulated genes.
204 Gene ontology pathway analyses revealed that a number of endocardium-initiated
205 signaling pathways were significantly downregulated in *Hdac3* KO MCECs (Supplemental
206 Figure 9A). Through DGE analysis, we found that growth factors including *Igf1, Tgfβ3,*
207 *Tgfβ2, Tgfβ1, Igf1, Cxcl12, Nrg1 and Vegfβ* were significantly downregulated in *Hdac3*
208 KO MCECs (Supplemental Figure 9B). We attempted to validate these results at the
209 protein level by western blot. Surprisingly, we found that only TGFβ3 protein expression
210 was significantly decreased in *Hdac3* KO MCECs as compared to *Hdac3* EV MCECs
211 (Supplemental Figure 9C), and thus we chose TGFβ3 to pursue further. Interestingly,

212 TGFβ3 was also significantly decreased when the deacetylase activity of HDAC3 was
213 inhibited by RGFP966 (a HDAC3 selective inhibitor) treatment (Figure 3C and
214 Supplemental Figure 9D). To assess *Tgfβ3* expression in E11.5 CECs, we sorted Tie2-
215 derived population from *Hdac3*^{tko} (*Hdac3*$^{f/f}$*; Tie2-Cre/+; R26*$^{eYFP/+}$) and CTL (*Hdac3*$^{f/+}$*;*
216 *Tie2-Cre/+; R26*$^{eYFP/+}$) hearts by performing fluorescence activated cell sorting on YFP
217 signal (Supplemental Figure 10). We found that *Tgfβ3* mRNA level was also significantly
218 downregulated in E11.5 *Hdac3* KO CECs compared to littermate CTL CECs (Figure 3D).
219 TGFβ3 downregulation in E11.5 *Hdac3*^{tko} hearts was further validated at the protein level
220 by western blot (Figure 3E). Next, we determined whether TGFβ3 deficiency in *Hdac3*
221 KO MCECs contributed to the CM proliferation deficit following *Hdac3* KO supernatant
222 treatment. First, we quantified TGFβ3 and found that it was significantly decreased in the
223 supernatants from *Hdac3* KO MCECs compared to that from *Hdac3* EV MCECs (Figure
224 3F). To determine whether TGFβ3 is an essential secretory component of MCEC
225 supernatants in stimulating CM proliferation, we generated *Tgfβ3* KO MCECs using
226 CRISPR-Cas9 gene editing technology (Supplemental Figure 12A). We found that *Tgfβ3*
227 KO significantly decreased the capacity of MCEC supernatants to induce CM proliferation
228 (percentage of Ki67+GFP+/GFP+ CMs) compared to CTL MCEC supernatant
229 (Supplemental Figure 12B). Further, we found that *Tgfβ3* KO significantly compromised
230 the capacity of MCEC supernatants in supporting myocardial trabeculation and
231 compaction when treating *ex vivo* cultured E11.5 CTL hearts with *Tgfβ3* KO MCEC
232 supernatants as compared to control MCEC supernatants (Supplemental Figure 12C).
233 These results altogether suggest that endocardial TGFβ3 is critical for myocardial growth.
234 Next, we evaluated CM proliferation after we supplemented *Hdac3* KO supernatants with

235 recombinant mouse TGFβ3 protein. Strikingly, TGFβ3 supplementation successfully
236 rescued CM proliferation defects by *Hdac3* KO supernatant treatment (Figure 3G).
237 Further, we found that TGFβ3 supplementation also rescued myocardial growth deficit in
238 *ex vivo* cultured E11.5 *Hdac3*^{tko} hearts (Supplemental Figure 13). These results suggest
239 that cardiac endothelial HDAC3 supports myocardial growth by inducing *Tgfβ3*
240 expression.
241
242 **Cardiac endothelial HDAC3 induces *Tgfβ3* expression through repressing**
243 **microRNA (miR)-129-5p.**
244 Recently, we reported that HDAC3 regulates growth factors by modulating the miR
245 pathway in the developing epicardium[26]. To identify the potential HDAC3 downstream
246 miR targets in CECs, we performed miR sequencing in *Hdac3* KO and EV MCECs.
247 Through DGE analyses, we found that 5 miRs were significantly upregulated in *Hdac3*
248 KO MCECs (Figure 4A) (cutoff threshold: Log2 fold change greater than 1.5 and adjusted
249 $P<0.01$). To identify which miR(s) may regulate *Tgfβ3* expression, we treated MCECs
250 with mimics of each of the 5 miRs and found that treatment with miR-129-5p mimics
251 significantly inhibited the expression of *Tgfβ3* (Figure 4B). This finding was validated by
252 western blot (Figure 4C). We further validated the upregulation of miR-129-5p in both
253 *Hdac3* KO MCECs and E11.5 *Hdac3*^{tko} hearts (Figure 4D and 4E). Interestingly, miR-
254 129-5p was similarly significantly upregulated when the deacetylase activity of HDAC3 is
255 inhibited by RGFP966 treatment (Figure 4D), suggesting that the inhibition of miR-129-
256 5p expression by HDAC3 is deacetylase dependent. To determine whether miR-129-5p
257 upregulation in MCECs has potential impact on myocardial growth, we treated cultured

258 *Tnnt2*$^{nGFP/+38}$ CMs or cultured whole E11.5 wildtype hearts with supernatants from
259 MCECs transfected with either miR-129-5p mimics or scramble RNAs. We found that
260 miR-129-5p supernatant treatment significantly decreased its capacity to induce CM
261 proliferation and myocardial growth (Supplemental Figure 14). Lastly, to determine
262 whether HDAC3 induces *Tgfβ3* expression through repressing miR-129-5p, we knocked
263 down miR-129-5p by miRZip lentivirus in *Hdac3* KO MCECs. Remarkably, miR-129-5p
264 knockdown significantly restored the TGFβ3 expression in *Hdac3* KO MCECs (Figure 4G).
265 Further, the supernatants from miR-129-5p knockdown *Hdac3* KO MCECs significantly
266 restored the CM proliferation promoting capacity from *Hdac3* KO MCEC supernatants
267 (Figure 4H). These results suggest that HDAC3 promotes the expression of TGFβ3
268 through repressing miR-129 in supporting trabecular myocardial growth (Figure 4I).

269 **Discussion**

270 Myocardial growth/expansion, one of the most critical cardiac developmental events, is
271 accompanied by two separate but closely associated processes: compaction and
272 trabeculation. Many forms of congenital heart disease are associated with abnormal
273 cardiac trabeculation and compaction[2, 3]. For proper myocardial development, besides
274 CMs, the surrounding non-CMs including endocardial cells can influence myocardial
275 growth by sending growth signals to the neighboring myocardia[39], as well as secreting
276 ECM proteins that serve as signal transmission media[2, 40]

277 Epigenetic regulation can define a tissue-specific and developmental stage-specific
278 transcription network during early heart development[41, 42], mainly achieved by
279 posttranslational modifications of histones, around which DNA winds. There are several
280 different types of histone modifications (e.g., methylation/demethylation,
281 acetylation/deacetylation, phosphorylation/dephosphorylation, ubiquitination/
282 deubiquitination). By alternating between any of these states, the associated genes can
283 be dynamically poised to be transcriptionally active/repressed. Histone deacetylases
284 (HDACs) are family of enzymes that remove acetyl groups from a lysine residue on a
285 histone, allowing the histones to wrap the DNA more tightly to repress gene expression.
286 Class I HDACs, includes HDAC3, are widely expressed, but play specific roles during
287 early embryogenesis and organogenesis[19]. Mesodermal or global KO of *Hdac3* results in
288 myogenic defects and early embryonic lethality[22, 43]. Interestingly, specific deletion of
289 *Hdac3* in the myocardium does not generate cardiac morphogenic phenotypes during
290 early heart development, but rather compromises cardiac function at later postnatal
291 stages[43, 44]. These early findings suggest that the function of HDAC3 in nonmyocyte

292 compartments may be critical for early cardiac morphogenesis and myocardial
293 development. Our recent work demonstrated that epicardial HDAC3 is critical for driving
294 myocardial compact wall expansion[26]. Our current study suggests that endocardial
295 HDAC3 is important for myocardial trabeculation: endothelial/endocardial deletion of
296 *Hdac3* resulted in hypotrabeculation (Figure 1 and Supplemental Figure 4). We note that
297 *Tie2-Cre* turns on around E8.0-8.5 in all endothelial cells[29], whereas *Nfatc1*$^{Cre/+}$ is active
298 around E9.5 only in endocardial cells[30] and only achieves efficient *Hdac3* deletion by
299 E14.5 likely due to inefficient IRES-mediated Cre transcription[45] (Supplemental Figure 4).
300 Nonetheless, these two deletion models generated similar cardiac phenotypes of
301 hypotrabeculation, although we did observe differences in the severity of the myocardial
302 phenotypes and time of lethality, which we attribute to the different temporal and spatial
303 activities and/or efficiencies of these two Cres. We also observed that both E12.5
304 *Hdac3*^{tko} and E14.5 *Hdac3*^{nko} hearts exhibited thin compact wall phenotype. This is likely
305 attributable to *Hdac3* deficiency in the subepicardial endothelial population which form
306 coronary arteries invading and supporting compact wall[46]. This late thin compact wall
307 phenotype is also consistent with the similar phenotype resulted from epicardial deletion
308 of *Hdac3*[26]. An earlier report of conditional deletion of *Hdac3* in endothelial cells using a
309 different *Tie2-Cre* driver primarily targeting hemogenic endothelial cells[27] resulted in mid-
310 gestational lethality (E14.5) presenting predominantly a lymphovenous and lymphatic
311 valve malformation phenotype[47]. However, it is unknown what phenotypes were present
312 in the myocardium in that study as none were reported. Nonetheless, we deemed it
313 inapplicable to evaluate potential lymphatic valve phenotypes in our pan-endothelial
314 *Hdac3* KO embryos since these mice died around E12.5 (Supplemental Table 1), while

315 lymphovenous and lymphatic valve formation starts at E13.5[48]. However, it is interesting
316 to note that the role of HDAC1 and HDAC2 in the developing endocardium appears to be
317 dispensable, as deletion of either *Hdac1* or *Hdac2* by *Tie2-Cre* do not elicit apparent
318 cardiac phenotypes[24]. These results suggest that HDAC3 plays distinctive roles from
319 HDAC1 and HDAC2, although they share high homology and are grouped in the same
320 HDAC subfamily[19].
321 TGFß signaling is involved in many processes during early heart development such as
322 ECM production, endothelial to mesenchymal transition, and myogenesis[11, 49, 50, 51].
323 Specifically, TGFß signaling plays a critical role during early cardiac myocardial
324 development[52, 53, 54, 55]. For instance, knockout of either TGFß2 or TGFß3 results in
325 hypoplastic ventricular myocardium[15], while TGFß1 is reported to inhibit CM
326 proliferation[55, 56], suggesting the complexity and specificity of TGFß isoforms during early
327 heart development. In the current study, we found that TGFß3 expression was
328 significantly decreased in *Hdac3* deleted endocardium, and TGFß3 treatment vigorously
329 stimulated CM proliferation (Figure 3). Interestingly, inhibition of deacetylase activity of
330 HDAC3 alone significantly decreased TGFß3 expression. Further, supplementation of
331 TGFß3 to cardiac endothelial *Hdac3* KO secretome significantly rescued CM proliferation
332 and myocardial growth defect (Figure 3), suggesting that cardiac endothelial HDAC3
333 supports trabeculation through inducing TGFß3 in a deacetylase dependent manner.
334 Interestingly, HDAC3 is also reported to inhibit TGFß1 expression in the second heart
335 field development in a deacetylase independent manner[23], whereas HDAC3 deteriorates
336 colorectal cancer progression by inducing TGFß1 through inhibiting miR-296[57]. These

337 divergent findings illustrate that HDAC3 can either promote or inhibit TGFß signaling
338 pathway through different molecular mechanisms in a tissue/cell dependent manner.
339 Besides functioning as growth signals to CMs, TGFß signaling is predominantly known
340 for its induction on ECMs[50, 58]. During early heart development, ECM is mainly secreted
341 from endocardium and mediates signal transduction from endocardium to myocardium
342 supporting trabeculation[57]. Our scRNA-Seq data revealed that ECM is significantly down
343 regulated in *Hdac3* endothelial KO hearts (Figure 2). P4ha3, a major enzyme for collagen
344 synthesis[59] and a TGFß downstream target[60], was also significantly decreased in *Hdac3*
345 endothelial knockout hearts (Figure 2). These results suggest that ECM downregulation
346 may be secondary to decreased TGFß signaling to contribute to the hypotrabeculation
347 phenotypes in *Hdac3* endothelial/endocardial knockout hearts.
348 We identified that HDAC3 suppresses miR-129-5p in inducing TGFß3 (Figure 4). miR-
349 129-5p plays important roles in cancer by either promoting or inhibiting tumorigenesis
350 through regulating a variety of downstream targets and pathways[61, 62]. Several studies
351 have shown that miR-129-5p protects adult hearts from ischemia/reperfusion injuries[63,
352 64], while another study demonstrated that treating cultured H9c2 with HDAC pan-inhibitor
353 Trichostatin A results in decreased CM proliferation with enhanced miR-129-5p
354 expression[65]. This is consistent with our current findings in the developing endocardium
355 (Figure 4). In our recent study, we found that HDAC3 induces the expression of IGF2 and
356 FGF9 by suppressing miR-322/503 in the developing epicardium[26]. Again, these findings
357 altogether suggest that HDAC3 can induce different sets of growth signals by switching
358 their downstream miR targets in a tissue/cell context dependent manner. On the other
359 hand, HDAC3, as a histone modifier, may have many downstream targets that participate

360 in other signaling pathways and exert various other biological effects. For instance,
361 several Wnt ligands (e.g., *Wnt4, Wnt5a,* and *Wnt11*) and Hedgehog signaling
362 components (*Smo, EVC,* and *Gli2*) were also significantly downregulated in *Hdac3* KO
363 MCECs. The disruption of these signaling pathways may affect cell adhesion, migration
364 and ciliogenesis[66, 67], thus also contribute to the overall *Hdac3*^{tko} cardiac phenotypes. We
365 will be actively investigating these possibilities in our future studies.
366 In summary, our current study demonstrates that endocardial HDAC3 promotes
367 myocardial trabeculation by inducing TGFß signaling through repressing miR-129-5p
368 during early heart development. This finding, along with others, exemplifies the
369 importance of endocardial signaling for driving myocardial morphogenesis, and thus
370 provides new insights on the pathogenesis of congenital heart disease. The dual
371 epigenetic inhibition mechanism may be leveraged in some other contexts such as adult
372 heart repair/regeneration.

373 **Methods**

374 ***Mice***

375 *Hdac3*$^{flox/+}$, *Tie2-Cre*, *Nfatc1*$^{Cre/+}$, *R26*^{eYFP} and *Tnnt2*$^{nGFP/+}$ mice were previously
376 described[27, 30, 38, 68, 69]. B6.Cg-Tg(*Tek-cre*)12Flv/J (abbreviated as *Tie2-Cre* in this
377 manuscript), *Hdac3*$^{flox/+}$, and *R26*^{eYFP} mice are available at the Jackson Laboratory (Stock
378 numbers: #004128, #024119 and #006148, respectively). All animal protocols were
379 approved by the Nationwide Children's Institutional Animal Care and Use Committee
380 (IACUC #AR22-00194).

381

382 ***Histology and immunofluorescence staining***

383 All embryo specimens were fixed in 4% paraformaldehyde overnight, dehydrated through
384 an ethanol series, paraffin embedded, and sectioned (6-7μm). Primary antibodies (Major
385 Resources Table) were incubated at 4°C overnight and secondary antibodies (Alexa 488
386 or Alexa 555, Thermo Fisher Scientific, Waltham, MA) were incubated at room
387 temperature for one hour. Stained slides were imaged on a Zeiss LSM 710 confocal
388 Microscope or a Leica DM6 fluorescence microscope. Epifluorescence and gross images
389 of embryos were imaged on a Leica M205 FCA stereo fluorescence microscope. The
390 number of phosphor-Histone 3 (p-H3)+ cells, Bromodeoxyuridine (BrdU)+ cells, and
391 TUNEL+ cells was quantified using ImageJ software.

392

393 ***Embryonic cardiomyocyte (CM) culture and proliferation assessment***

394 E13.5 ventricular CMs were isolated from dissected embryonic hearts and cultured as
395 previously described[70]. To assess cell proliferation, CMs were fixed with 4%

396 paraformaldehyde and stained with Ki67 or p-H3 antibody followed by Alexa 594-
397 conjugated secondary antibody (Thermo Fisher Scientific, Waltham, MA). The
398 immunostaining was visualized and imaged on a Keyence BZ-X800 microscope. The
399 percentages of Ki67+GFP+/GFP+, p-H3+GFP+/GFP+ and total number of GFP+ CMs
400 were quantified using ImageJ software.

401

402 ***Endothelial cell culture, transient transfection, lentiviral infection, and luciferase***
403 ***assay***

404 Mouse cardiac endothelial cells (MCECs) were purchased from Cedarlane Labs
405 (Catalogue #CLU510, Burlington, NC). MCECs were cultured in 10% fetal bovine serum
406 (FBS) supplemented DMEM at 37°C in a humidified incubator with 5% CO_2. To generate
407 stable *Hdac3* KO MCECs, as previously described[26], we cloned *Hdac3* sgRNA into
408 lentiCRISPR v2 vector (Addgene #52961; Watertown, MA). Seventy-percent confluent
409 Lenti-X™ 293T cells (Takara Bio USA, Inc., Mountain View, CA) were transfected with
410 *Hdac3* lentiviral plasmids (*Hdac3* KO or empty vector control [EV])[26], *Tgfβ3* lentiviral
411 plasmids (*Tgfβ3* KO or empty vector control [EV]) were purchased from VectorBuilder,
412 PsPAX2 (Addgene #12260) and PMD2G (Addgene #12259). Seventy-two hours after
413 transfection, supernatants containing lentivirus were collected and filtered through a
414 40μm cell strainer. Mir-129-5p, miR-129b-3p, miR-129b-5p, mir-129-2-3p, miR-708-3p
415 mimics and scramble control mimics were custom-ordered from ThermoFischer Scientific
416 (Waltham, MA). MCECs were transfected with miRNA mimics or control mimics (30 pmol)
417 using Lipofectamine RNAiMAX (Thermo Fisher Scientific, Waltham, MA). 72 hours after
418 miR mimics treatment, supernatants were collected. miRZip anti-miR precursor

419 constructs for miRZip-129-5p and pGreenPuro Scramble Hairpin control constructs were
420 purchased from System Biosciences (Palo Alto, CA), and lentiviruses were generated
421 according to the manufacturer's protocol.
422
423 ***Ex Vivo embryonic heart culture***
424 E11.5 embryonic hearts were dissected in cold PBS, and then cultured in DMEM/F-12
425 media (Thermofisher Scientific, Waltham, MA, #11039021). Embryonic cardiac explants
426 were treated with either TGFß3 recombinant protein (Sigmal Aldrich, Saint Louis, MO,
427 #SRP6552, final concentration: 250 ng/ml), *Tgfß3* KO MCEC supernatants, miR-129-5p
428 mimics-treated MCEC supernatants and their corresponding control media or control
429 MCEC supernatants for 24 hours at 37 °C. Hearts were then fixed in 4%
430 paraformaldehyde overnight at 4 °C and processed for paraffin embedding and
431 sectioning.
432
433 ***Fluorescence activated cell sorting of YFP+ Tie2 derivative cardiac cells***
434 E11.5 hearts were dissected and dissociated with 0.5% trypsin–EDTA into a single cell
435 suspension. Cell suspension was washed with PBS and YFP+ cells were gated using
436 their autofluoresence signal and sorted and using a BD Influx cell sorter (BD Biosciences).
437 The harvested YFP+ cells were used for subsequent gene expression analysis.
438
439 ***RNA isolation, quantitative real-time PCR (qRT-PCR), and bulk RNA-Seq***
440 MCECs and embryonic day (E) 11.5 hearts were used for RNA isolation. E11.5 hearts
441 were microdissected in cold PBS and snap frozen in liquid nitrogen. The RNeasy Plus

442 Mini Kit (QIAGEN, Germantown, MD) was used to extract total RNA, and cDNAs were
443 generated using the Superscript III kit (Thermo Fisher Scientific, Waltham, MA). To detect
444 mRNA, SYBR Green qRT-PCR was performed. PCR primers for genes of interest are
445 listed in Major Resources Table. To perform mature microRNA expression analyses,
446 purified total RNAs were converted to cDNAs using TaqMan™ MicroRNA Reverse
447 Transcription Kit (Catalogue #4366596, Thermo Fisher Scientific). qRT-PCR reactions
448 were run on StepOne Plus Real-Time PCR System (Applied Biosystems, Waltham, MA).
449 The probe sequences for mmu-miR-129-5p and U6 snRNA were purchased from Thermo
450 Fisher Scientific. For bulk RNA and miRNA-Sequencing, samples were prepared
451 following the provider's guidelines (Novogene Corporation Inc, Sacramento, CA) and
452 sequenced on an Illumina NextSeq500 (San Diego, CA). Sequencing reads were aligned
453 to the UCSC mm10 reference genome using tophat2 and bowtie2 in R. Differential
454 expression of transcripts was calculated using the cufflinks suite in R analyses.
455
456 ***Single cell RNA-Sequencing (scRNA-seq)***
457 E11.5 heart tissues were dissected in cold PBS and digested with 0.25% trypsin at 37°C
458 for 15 minutes. Digested cardiac cells were filtered with 70 μm cell strainers to remove
459 remaining clumps. Subsequently, 10,000 live cells were captured with Chromium Next
460 GEM Single Cell 3' Reagent Kits v3.1 (10X Genomics, Pleasanton, CA) following
461 manufacturer's instructions. Briefly, single cells were partitioned into nanoliter-scale Gel
462 Beads-in-emulsion (GEMs) using Chromium Next GEM Chip G in the chromium controller.
463 Immediately following GEM generation, the Gel Bead was dissolved, primers were
464 released, and co-partitioned cell was lysed, and its mRNA were reverse transcribed into

465 barcoded cDNA. After further cleanup and amplification, the cDNA was enzymatically
466 fragmented and amplified via PCR to generate sufficient mass for library construction.
467 After end repair, A-tailing, adaptor ligation and sample index PCR, the library comprised
468 constructs containing the sample index, UMI sequences, barcode sequences, and
469 Illumina standard sequencing primers P5 and P7 at both ends. The library was sequenced
470 with Illumina NextSeq S4 platform to a sequencing depth of 140-270 million reads per
471 sample. Reads were aligned to the Ensembl 104 mouse reference genome including the
472 sequence for eYFP as a separate contig using STARsolo (version 2.7.10b)[71]. The
473 resulting count tables (cells x genes) were converted into Annotated Data (anndata)
474 format for analysis in Python. For quality control, all cells with less than 1500 or more than
475 9000 genes expressed were excluded. Additionally, cell doublets were filtered out using
476 the Scrublet method[72]. Gene counts were normalized per cell to a total target sum and
477 transformed using log1p. Highly variable genes were identified using the Seurat method[73]
478 and these genes were utilized for dimension reduction with PCA. Finally, cell embedding
479 was performed with the UMAP algorithm (umap-learn version 0.5.3) and cells were
480 clustered using leiden (leidenalg version 0.9.1) with resolution 0.2. Scoring of trabecular
481 and compact CM subtypes was performed using 'score_genes' and differentially
482 expressed genes between groups were obtained using 'rank_genes_groups', both
483 methods from the SCANPY package[74].
484
485 ***Western blotting***
486 Cell or tissue lysates were prepared in lysis buffer (20 mM Tris-HCl [pH 7.5], 15 mM NaCl,
487 1 mM Na_2EDTA, 1 mM EGTA, 1% Triton X-100, 1 µg/ml leupeptin, 2.5 mM sodium

488 pyrophosphate, 1 mM Na_3VO_4, and 1 mM β-glycerophosphate) with protease inhibitor
489 cocktail (Roche, Indianapolis, IN) and 1 mM phenylmethylsulfonyl fluoride. Protein
490 samples were resolved on 4–12% SDS-PAGE acrylamide gels before transferring to
491 polyvinylidene fluoride membranes. Primary antibodies were visualized by
492 chemiluminescence using HRP-conjugated secondary antibodies. Antibodies are listed
493 in Major Resources Table. Western blots were normalized to loading controls and
494 densitometric analysis was performed using Image J software.
495
496 ***Statistical analysis***
497 All experiments were independently repeated at least three times, and the number of
498 samples (n) is stated in figure legends. Results are reported as the mean ± SD. For
499 statistical analyses, normal distribution of data was assessed by Shapiro-Wilk's test
500 (when n≥6). For data with small sample size (n<6), non-parametric tests were applied.
501 For parametric data with normal distribution, the statistical significance of the difference
502 between means was assessed using the unpaired two tailed Student's t-test between two
503 groups and the Tukey or Dunnett post hoc test for one-way ANOVA. For non-parametric
504 data or data with small sample size (n<6), the Mann-Whitney U test and Kruskal-Wallis
505 test for one-way ANOVA followed by the Dunn post hoc test were performed for
506 comparisons between two groups. Specific statistical tests are stated in figure legends.
507 RNA-seq data were background-corrected, variance-stabilized, normalized, and count
508 matrix extracted through quality control using lumi package for the R programming
509 language (http://bioconductor.org/packages/release/bioc/html/lumi.html). Differential
510 expression analysis was performed using DESeq2 R package

511 (https://bioconductor.org/packages/release/bioc/html/DESeq2. html). The resulting *p*-
512 values were adjusted using the Benjamini and Hochberg's approach for controlling the
513 False Discovery Rate (FDR)[75]. Genes or miRs with an adjusted *p*-value<0.05 found by
514 DESeq2 were assigned as differentially expressed. Gene ontology (GO) enrichment
515 analyses were performed using the Database for Annotation, Visualization and Integrated
516 Discovery (DAVID) bioinformatics resources (https://david.ncifcrf.gov/). For relative gene
517 expression analysis of qRT-PCR data, the expression of a gene of interest relative to an
518 internal loading control gene was calculated using the comparative CT method (-ΔΔCT)[76].
519 The relative protein expression on western blots was quantified by densitometry, Fold
520 changes for relative gene or protein expression were derived through division of values
521 in the experimental group by the mean values from the control group. *P*-value<0.05 was
522 considered statistically significant. All statistical analyses were performed using
523 GraphPad Prism 8 (GraphPad Prism software, Inc). The images with the value closest to
524 the mean value were selected as representative images.
525

526 **Data Availability**

527 All data associated with this study are present in the main text or the supplementary
528 materials. The scRNA-seq, RNA-seq and miRNA-seq data generated in this study have
529 been deposited in the GEO database under accession code GSE229661. All raw data
530 are available from the authors upon reasonable request.

531

532 **References:**

533 1. Zaidi S, Brueckner M. Genetics and Genomics of Congenital Heart Disease. *Circulation*
534 *research* **120**, 923-940 (2017).
535
536 2. Qu X, Harmelink C, Baldwin HS. Endocardial-Myocardial Interactions During Early
537 Cardiac Differentiation and Trabeculation. *Front Cardiovasc Med* **9**, 857581 (2022).
538
539 3. Wu M. Mechanisms of Trabecular Formation and Specification During Cardiogenesis.
540 *Pediatric cardiology* **39**, 1082-1089 (2018).
541
542 4. Lin W, Li D. Zinc and Zinc Transporters: Novel Regulators of Ventricular Myocardial
543 Development. *Pediatric cardiology* **39**, 1042-1051 (2018).
544
545 5. Zhang W, Chen H, Qu X, Chang CP, Shou W. Molecular mechanism of ventricular
546 trabeculation/compaction and the pathogenesis of the left ventricular noncompaction
547 cardiomyopathy (LVNC). *American journal of medical genetics Part C, Seminars in*
548 *medical genetics* **163C**, 144-156 (2013).
549
550 6. Zhang H, Lui KO, Zhou B. Endocardial Cell Plasticity in Cardiac Development, Diseases
551 and Regeneration. *Circulation research* **122**, 774-789 (2018).
552
553 7. Andries LJ, Sys SU, Brutsaert DL. Morphoregulatory interactions of endocardial
554 endothelium and extracellular material in the heart. *Herz* **20**, 135-145 (1995).
555

556 8. Camenisch TD*, et al.* Disruption of hyaluronan synthase-2 abrogates normal cardiac
557 morphogenesis and hyaluronan-mediated transformation of epithelium to mesenchyme. *J*
558 *Clin Invest* **106**, 349-360 (2000).
559
560 9. Hatano S*, et al.* Versican/PG-M is essential for ventricular septal formation subsequent to
561 cardiac atrioventricular cushion development. *Glycobiology* **22**, 1268-1277 (2012).
562
563 10. Chen JL, Colgan TD, Walton KL, Gregorevic P, Harrison CA. The TGF-beta Signalling
564 Network in Muscle Development, Adaptation and Disease. *Adv Exp Med Biol* **900**, 97-131
565 (2016).
566
567 11. Sorensen DW, van Berlo JH. The Role of TGF-beta Signaling in Cardiomyocyte
568 Proliferation. *Curr Heart Fail Rep* **17**, 225-233 (2020).
569
570 12. Zhang Y, Yang X. The Roles of TGF-beta Signaling in Cerebrovascular Diseases. *Front*
571 *Cell Dev Biol* **8**, 567682 (2020).
572
573 13. Moustakas A, Heldin CH. Non-Smad TGF-beta signals. *J Cell Sci* **118**, 3573-3584 (2005).
574
575 14. Zhang YE. Non-Smad pathways in TGF-beta signaling. *Cell Res* **19**, 128-139 (2009).
576
577 15. Azhar M*, et al.* Transforming growth factor beta in cardiovascular development and
578 function. *Cytokine Growth Factor Rev* **14**, 391-407 (2003).
579

580 16. Koo SH, Cunningham MC, Arabshahi B, Gruss JS, Grant JH, 3rd. The transforming growth
581 factor-beta 3 knock-out mouse: an animal model for cleft palate. *Plast Reconstr Surg* **108**,
582 938-948; discussion 949-951 (2001).
583
584 17. Sanford LP*, et al.* TGFbeta2 knockout mice have multiple developmental defects that are
585 non-overlapping with other TGFbeta knockout phenotypes. *Development* **124**, 2659-2670
586 (1997).
587
588 18. Kulkarni AB, Karlsson S. Transforming growth factor-beta 1 knockout mice. A mutation in
589 one cytokine gene causes a dramatic inflammatory disease. *Am J Pathol* **143**, 3-9 (1993).
590
591 19. Haberland M, Montgomery RL, Olson EN. The many roles of histone deacetylases in
592 development and physiology: implications for disease and therapy. *Nature reviews*
593 *Genetics* **10**, 32-42 (2009).
594
595 20. Dsilva P, Pai P, Shetty MG, Babitha KS. The role of histone deacetylases in embryonic
596 development. *Mol Reprod Dev* **90**, 14-26 (2023).
597
598 21. Wang Z, Zhao YT, Zhao TC. Histone deacetylases in modulating cardiac disease and their
599 clinical translational and therapeutic implications. *Exp Biol Med (Maywood)* **246**, 213-225
600 (2021).
601
602 22. Bhaskara S*, et al.* Deletion of histone deacetylase 3 reveals critical roles in S phase
603 progression and DNA damage control. *Mol Cell* **30**, 61-72 (2008).
604

605 23. Lewandowski SL, Janardhan HP, Trivedi CM. Histone Deacetylase 3 Coordinates
606 Deacetylase-independent Epigenetic Silencing of Transforming Growth Factor-beta1
607 (TGF-beta1) to Orchestrate Second Heart Field Development. *The Journal of biological*
608 *chemistry* **290**, 27067-27089 (2015).
609
610 24. Janardhan HP, Milstone ZJ, Shin M, Lawson ND, Keaney JF, Jr., Trivedi CM. Hdac3
611 regulates lymphovenous and lymphatic valve formation. *J Clin Invest* **127**, 4193-4206
612 (2017).
613
614 25. Poleshko A*, et al.* Genome-Nuclear Lamina Interactions Regulate Cardiac Stem Cell
615 Lineage Restriction. *Cell* **171**, 573-587 e514 (2017).
616
617 26. Jang J*, et al.* Epicardial HDAC3 Promotes Myocardial Growth Through a Novel MicroRNA
618 Pathway. *Circulation research* **131**, 151-164 (2022).
619
620 27. Koni PA, Joshi SK, Temann UA, Olson D, Burkly L, Flavell RA. Conditional vascular cell
621 adhesion molecule 1 deletion in mice: impaired lymphocyte migration to bone marrow.
622 *The Journal of experimental medicine* **193**, 741-754 (2001).
623
624 28. de Lange WJ, Halabi CM, Beyer AM, Sigmund CD. Germ line activation of the Tie2 and
625 SMMHC promoters causes noncell-specific deletion of floxed alleles. *Physiol Genomics*
626 **35**, 1-4 (2008).
627
628 29. Kisanuki YY, Hammer RE, Miyazaki J, Williams SC, Richardson JA, Yanagisawa M. Tie2-
629 Cre transgenic mice: a new model for endothelial cell-lineage analysis in vivo. *Dev Biol*
630 **230**, 230-242 (2001).

631

632 30. Wu B*, et al.* Endocardial cells form the coronary arteries by angiogenesis through
633 myocardial-endocardial VEGF signaling. *Cell* **151**, 1083-1096 (2012).
634

635 31. Wu T*, et al.* PRDM16 Is a Compact Myocardium-Enriched Transcription Factor Required
636 to Maintain Compact Myocardial Cardiomyocyte Identity in Left Ventricle. *Circulation* **145**,
637 586-602 (2022).
638

639 32. Hassan MK, Kumar D, Patel SA, Dixit M. EEF1A2 triggers stronger ERK mediated
640 metastatic program in ER negative breast cancer cells than in ER positive cells. *Life Sci*
641 **262**, 118553 (2020).
642

643 33. Fish JE*, et al.* Dynamic regulation of VEGF-inducible genes by an ERK/ERG/p300
644 transcriptional network. *Development* **144**, 2428-2444 (2017).
645

646 34. Thornton S, Anand N, Purcell D, Lee J. Not just for housekeeping: protein initiation and
647 elongation factors in cell growth and tumorigenesis. *J Mol Med (Berl)* **81**, 536-548 (2003).
648

649 35. Anbara T, Sharifi M, Aboutaleb N. Endothelial to Mesenchymal Transition in the
650 Cardiogenesis and Cardiovascular Diseases. *Curr Cardiol Rev* **16**, 306-314 (2020).
651

652 36. Del Monte-Nieto G*, et al.* Control of cardiac jelly dynamics by NOTCH1 and NRG1 defines
653 the building plan for trabeculation. *Nature* **557**, 439-445 (2018).
654

655 37. Barbieri SS, Weksler BB. Tobacco smoke cooperates with interleukin-1beta to alter beta-
656 catenin trafficking in vascular endothelium resulting in increased permeability and

657 induction of cyclooxygenase-2 expression in vitro and in vivo. *FASEB J* **21**, 1831-1843
658 (2007).
659
660 38. Yan J*, et al.* A series of robust genetic indicators for definitive identification of
661 cardiomyocytes. *J Mol Cell Cardiol* **97**, 278-285 (2016).
662
663 39. Tian Y, Morrisey EE. Importance of myocyte-nonmyocyte interactions in cardiac
664 development and disease. *Circulation research* **110**, 1023-1034 (2012).
665
666 40. Silva AC, Pereira C, Fonseca A, Pinto-do OP, Nascimento DS. Bearing My Heart: The
667 Role of Extracellular Matrix on Cardiac Development, Homeostasis, and Injury Response.
668 *Front Cell Dev Biol* **8**, 621644 (2020).
669
670 41. Paige SL*, et al.* A temporal chromatin signature in human embryonic stem cells identifies
671 regulators of cardiac development. *Cell* **151**, 221-232 (2012).
672
673 42. Wamstad JA*, et al.* Dynamic and coordinated epigenetic regulation of developmental
674 transitions in the cardiac lineage. *Cell* **151**, 206-220 (2012).
675
676 43. Lewandowski SL, Janardhan HP, Trivedi CM. Histone Deacetylase 3 Coordinates
677 Deacetylase-independent Epigenetic Silencing of Transforming Growth Factor-beta1
678 (TGF-beta1) to Orchestrate Second Heart Field Development. *The Journal of biological*
679 *chemistry* **290**, 27067-27089 (2015).
680
681 44. Montgomery RL*, et al.* Maintenance of cardiac energy metabolism by histone deacetylase
682 3 in mice. *J Clin Invest* **118**, 3588-3597 (2008).

683

684 45. Artap S*, et al.* Endocardial Hippo signaling regulates myocardial growth and
685 cardiogenesis. *Dev Biol* **440**, 22-30 (2018).
686

687 46. Tian X*, et al.* Subepicardial endothelial cells invade the embryonic ventricle wall to form
688 coronary arteries. *Cell Res* **23**, 1075-1090 (2013).
689

690 47. Celikyurt U, Karauzum K, Sahin T, Agacdiken A, Vural A, Ural D. Association between
691 resolution of fragmented QRS and response to cardiac resynchronization therapy. *Ann*
692 *Noninvasive Electrocardiol* **20**, 126-131 (2015).
693

694 48. Yang Y, Oliver G. Development of the mammalian lymphatic vasculature. *J Clin Invest*
695 **124**, 888-897 (2014).
696

697 49. Conway SJ, Doetschman T, Azhar M. The inter-relationship of periostin, TGF beta, and
698 BMP in heart valve development and valvular heart diseases. *ScientificWorldJournal* **11**,
699 1509-1524 (2011).
700

701 50. Frangogiannis NG. Transforming growth factor-beta in myocardial disease. *Nat Rev*
702 *Cardiol* **19**, 435-455 (2022).
703

704 51. Lee JH, Massague J. TGF-beta in developmental and fibrogenic EMTs. *Semin Cancer*
705 *Biol* **86**, 136-145 (2022).
706

707 52. Chakrabarti M*, et al.* Transforming Growth Factor Beta3 is Required for Cardiovascular
708 Development. *J Cardiovasc Dev Dis* **7**, (2020).

709

710 53. Dunker N, Krieglstein K. Tgfbeta2 -/- Tgfbeta3 -/- double knockout mice display severe
711 midline fusion defects and early embryonic lethality. *Anat Embryol (Berl)* **206**, 73-83
712 (2002).

713

714 54. Kruithof BP, Kruithof-De-Julio M, Poelmann RE, Gittenberger-De-Groot AC, Gaussin V,
715 Goumans MJ. Remodeling of the myocardium in early trabeculation and cardiac valve
716 formation; a role for TGFbeta2. *Int J Dev Biol* **57**, 853-863 (2013).

717

718 55. Kodo K*, et al.* iPSC-derived cardiomyocytes reveal abnormal TGF-beta signalling in left
719 ventricular non-compaction cardiomyopathy. *Nat Cell Biol* **18**, 1031-1042 (2016).

720

721 56. Engelmann GL, Boehm KD, Birchenall-Roberts MC, Ruscetti FW. Transforming growth
722 factor-beta 1 in heart development. *Mech Dev* **38**, 85-97 (1992).

723

724 57. Li J*, et al.* HDAC3 deteriorates colorectal cancer progression via microRNA-296-
725 3p/TGIF1/TGFbeta axis. *J Exp Clin Cancer Res* **39**, 248 (2020).

726

727 58. Algeciras L, Palanca A, Maestro D, RuizdelRio J, Villar AV. Epigenetic alterations of
728 TGFbeta and its main canonical signaling mediators in the context of cardiac fibrosis. *J*
729 *Mol Cell Cardiol* **159**, 38-47 (2021).

730

731 59. Van Den Diepstraten C, Papay K, Bolender Z, Brown A, Pickering JG. Cloning of a novel
732 prolyl 4-hydroxylase subunit expressed in the fibrous cap of human atherosclerotic plaque.
733 *Circulation* **108**, 508-511 (2003).

734

735 60. Luo Y*, et al.* A novel profibrotic mechanism mediated by TGFbeta-stimulated collagen
736 prolyl hydroxylase expression in fibrotic lung mesenchymal cells. *J Pathol* **236**, 384-394
737 (2015).
738
739 61. Deng B, Tang X, Wang Y. Role of microRNA-129 in cancer and non-cancerous diseases
740 (Review). *Exp Ther Med* **22**, 918 (2021).
741
742 62. Xu S*, et al.* The Role of miR-129-5p in Cancer: A Novel Therapeutic Target. *Curr Mol*
743 *Pharmacol* **15**, 647-657 (2022).
744
745 63. Ma R, Chen X, Ma Y, Bai G, Li DS. MiR-129-5p alleviates myocardial injury by targeting
746 suppressor of cytokine signaling 2 after ischemia/reperfusion. *Kaohsiung J Med Sci* **36**,
747 599-606 (2020).
748
749 64. Xing J, Liu J, Liu J, Xu Z. miR-129-5p ameliorates ischemia-reperfusion injury by targeting
750 HMGB1 in myocardium. *Gen Physiol Biophys* **39**, 461-470 (2020).
751
752 65. Majumdar G, Raghow R. Trichostatin A induces a unique set of microRNAs including miR-
753 129-5p that blocks cyclin-dependent kinase 6 expression and proliferation in H9c2 cardiac
754 myocytes. *Mol Cell Biochem* **415**, 39-49 (2016).
755
756 66. Quadri N, Upadhyai P. Primary cilia in skeletal development and disease. *Exp Cell Res*
757 **431**, 113751 (2023).
758
759 67. Flaherty MP, Kamerzell TJ, Dawn B. Wnt signaling and cardiac differentiation. *Prog Mol*
760 *Biol Transl Sci* **111**, 153-174 (2012).

761

762 68. Mullican SE*, et al.* Histone deacetylase 3 is an epigenomic brake in macrophage
763 alternative activation. *Genes & development* **25**, 2480-2488 (2011).
764

765 69. Srinivas S*, et al.* Cre reporter strains produced by targeted insertion of EYFP and ECFP
766 into the ROSA26 locus. *BMC Dev Biol* **1**, 4 (2001).
767

768 70. Beall MC, Li D, Jang J. Isolation of Embryonic Cardiomyocytes and Cell Proliferation
769 Assay Using Genetically Engineered Reporter Mouse Model. *Bio Protoc* **13**, e4802 (2023).
770

771 71. Dobin A*, et al.* STAR: ultrafast universal RNA-seq aligner. *Bioinformatics* **29**, 15-21 (2013).
772

773 72. Wolock SL, Lopez R, Klein AM. Scrublet: Computational Identification of Cell Doublets in
774 Single-Cell Transcriptomic Data. *Cell Syst* **8**, 281-291 e289 (2019).
775

776 73. Satija R, Farrell JA, Gennert D, Schier AF, Regev A. Spatial reconstruction of single-cell
777 gene expression data. *Nat Biotechnol* **33**, 495-502 (2015).
778

779 74. Wolf FA, Angerer P, Theis FJ. SCANPY: large-scale single-cell gene expression data
780 analysis. *Genome Biol* **19**, 15 (2018).
781

782 75. Wang L, Feng Z, Wang X, Wang X, Zhang X. DEGseq: an R package for identifying
783 differentially expressed genes from RNA-seq data. *Bioinformatics* **26**, 136-138 (2010).
784

785 76. Schmittgen TD, Livak KJ. Analyzing real-time PCR data by the comparative C(T) method.
786 *Nature protocols* **3**, 1101-1108 (2008).

790 **Acknowledgments**

791 We thank Dr. Dennis Lewandowski in the Heart Center at the Nationwide Children's
792 Hospital for his critical reading and editing of the manuscript.

793

794 **Author contributions**

795 J.J. and D.L. conceived and designed the study, analyzed the experiments, wrote the
796 paper. M.B and M.L performed scRNA-Seq data analysis. Y.J.K and E.K. performed the
797 experiments. C.C. provided *Tnnt2*$^{nGFP/+}$ mice. V.G., J.J. and D.L. edited manuscript. All
798 authors reviewed the results and approved the final version of the manuscript.

799

800 **Competing Interests**

801 None.

802

803 **Sources of Funding**

804 This work was partially supported by the National Heart, Lung, and Blood Institute R01
805 grant HL153406 (D. L.), American Heart Association (AHA)-Career Development Award
806 23CDA1046244 and AHA-Innovative Project Award 23IPA1048560 (J. J.).

807

Figures and Figure legends

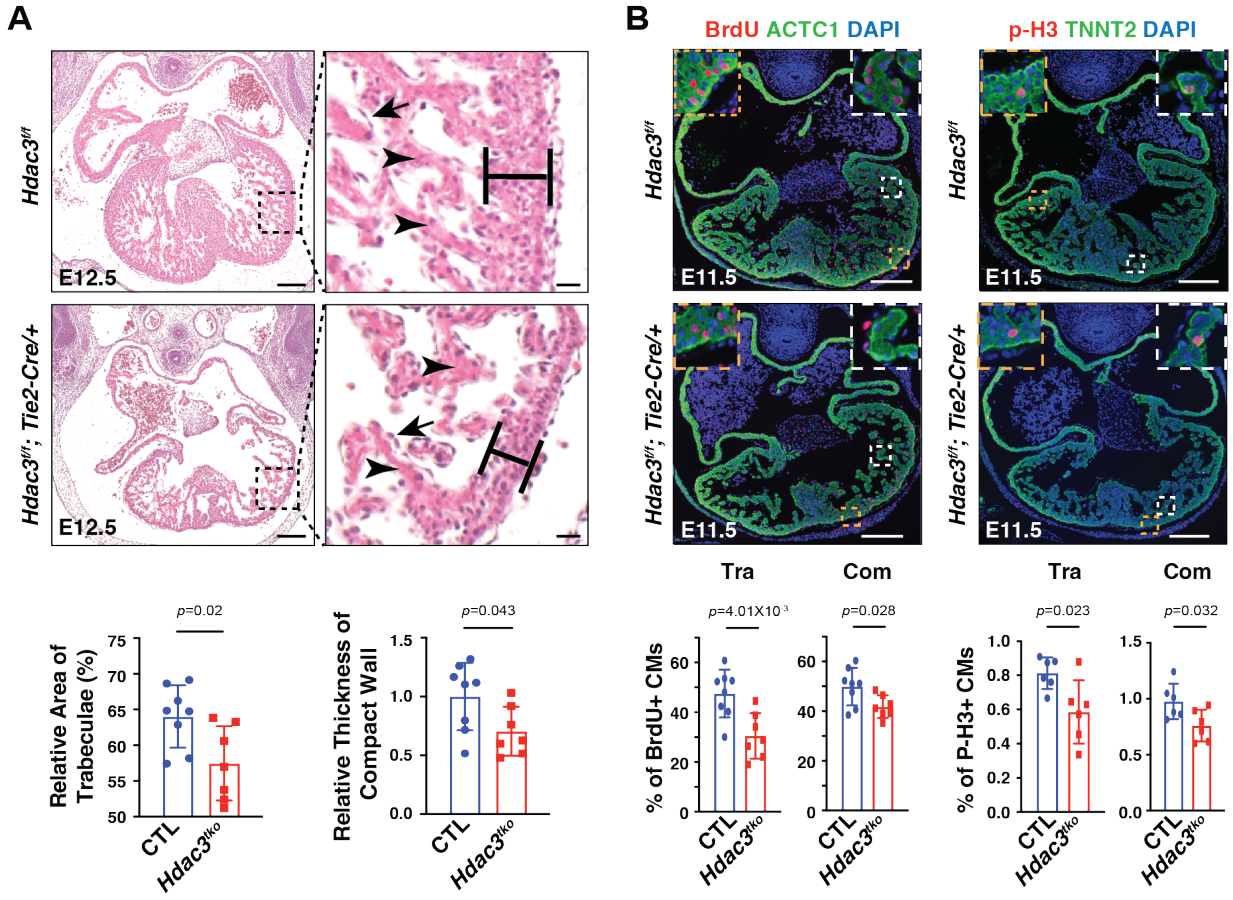

Figure 1. Endothelial specific deletion of *Hdac3* results in hypotrabeculation.

(A) Hematoxylin and eosin staining on cross sections of an E12.5 *Hdac3*^{tko} embryo (*Hdac3*$^{f/f}$*; Tie2-Cre/+*) and a littermate control (CTL) embryo (*Hdac3*$^{f/f}$). Arrows mark endocardium and arrowheads point to trabeculae. Quantifications are shown on the bottom (CTL: n=8, *Hdac3*^{tko}: n=7). Scale bars, 200 μm (main panels) and 25 μm (insets). **(B)** Decreased cardiomyocyte (CM) proliferation in E11.5 *Hdac3*^{tko} hearts. Immunofluorescence staining of Bromodeoxyuridine/5-bromo-2'-deoxyuridine (BrdU) and phospho-Histone H3 (p-H3) staining. High-power Images in the trabecular myocardium (Tra) and in the compact myocardium (Com) are highlighted in white and yellow boxes respectively. Scale bars, 200 μm. Quantification of proliferation index in the trabecular

820 and compact myocardium respectively are shown on the bottom. BrdU (CTL: n=8,
821 *Hdac3*^{tko}: n=7); p-H3 (n=6 in each group). *P*-values were determined by unpaired two
822 tailed Student's *t*-test.
823

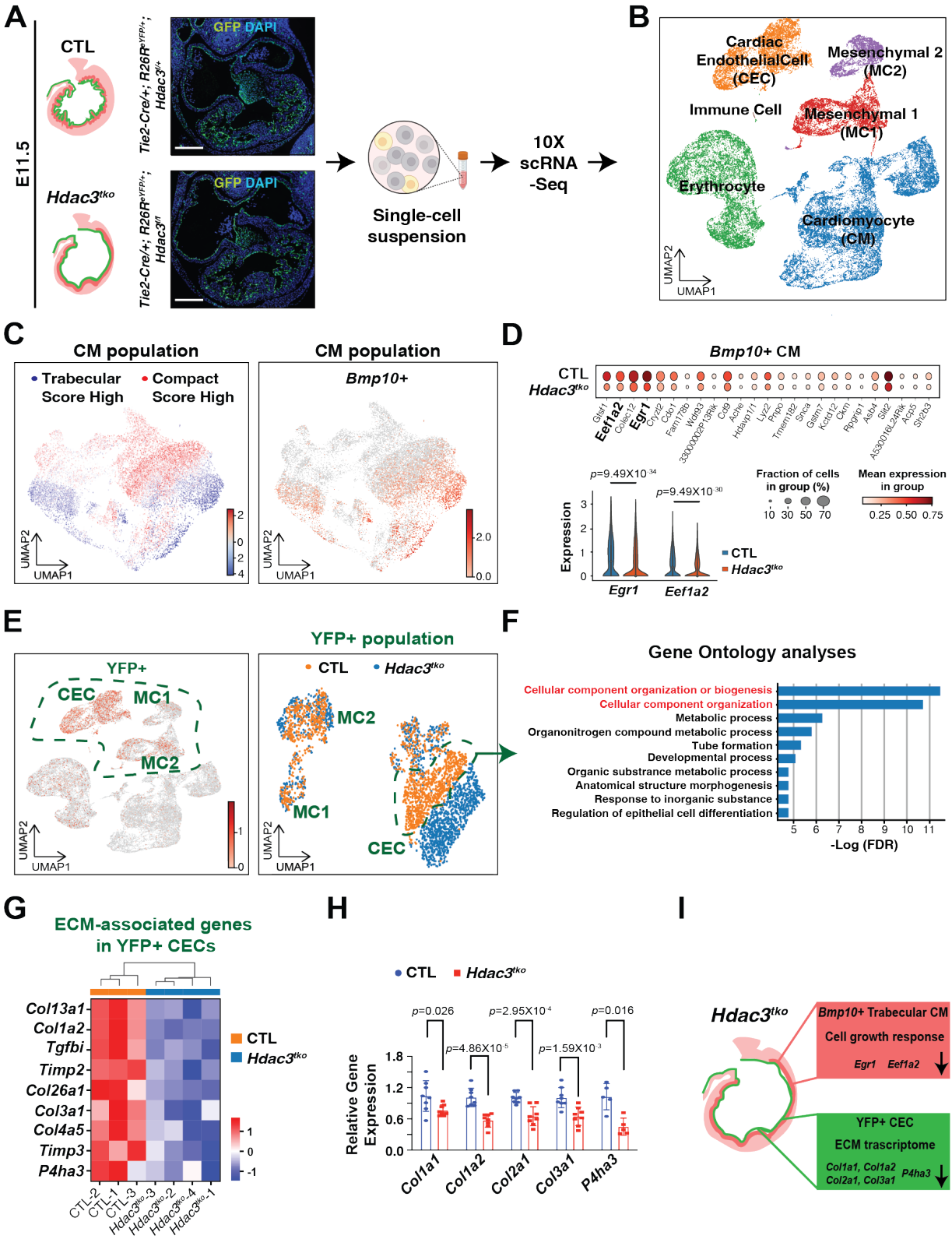

824 **Figure 2. Single-cell RNA sequencing reveals decreased expression of ECM genes**

825 **in *Hdac3*^{tko} hearts.**

826 **(A)** Schematic workflow of scRNA-Seq experimental design. Representative micrographs
827 of GFP immunofluorescence staining of E11.5 *Hdac3*^{tko} embryo (*Hdac3*$^{f/f}$*; Tie2-Cre/+;*
828 *R26R*$^{eYFP/+}$) and a littermate control (CTL) embryo (*Hdac3*$^{f/+}$*; Tie2-Cre/+; R26R*$^{eYFP/+}$).
829 Scale bars, 250 μm. **(B)** UMAP visualization of cell populations in an E11.5 control heart.
830 **(C)** Trabecular and compact cardiomyocyte (CM) score were calculated within *Tnni*+ CM
831 population. Left UMAP showed CMs split into a lower cluster that has a high trabecular
832 score, and an upper cluster that has a high compact score. Right UMAP shows the
833 expression level of *Bmp10*+ per cell. **(D)** Dot plots of differentially expressed genes in
834 *Hdac3*^{tko} and CTL trabecular clusters. Violin plots of expression of *Egr1* and *Eef1a2* in
835 *Hdac3*^{tko} and CTL trabecular clusters. **(E)** The UMAP on the left shows that YFP+ cells
836 are distributed in cardiac endothelial cell (CEC, *Cdh*+), mesenchymal cell 1 (MC1,
837 *Pdgfra*+), and mesenchymal cell 2 (MC2, *Dcn*+) clusters. The overlapping UMAPs of
838 *Hdac3*^{tko} and CTL YFP+ cells are shown on the right. **(F)** Gene Ontology pathway analysis
839 of top marker genes in CTL-specific YFP+ CEC cluster (Cut off value: -log (FDR)>5). **(G)**
840 Heatmap of extracellular matrix (ECM) associated genes in E11.5 *Hdac3*^{tko} and CTL
841 hearts. Data were extracted from YFP+ CEC clusters in the scRNA-Seq dataset. **(H)** qRT-
842 PCR analysis of *Col1a1*, *Col1a2*, *Col2a1*, *Col3a1* and *P4ha3* in E11.5 *Hdac3*^{tko} heart as
843 compared to CTL hearts (n=8 in each group for *Col1a1*, *Col1a2*, *Col2a1* and *Col3a1,* n=5
844 in each group for *P4ha3*). *P*-values were determined by unpaired two tailed Student's *t*-
845 test. (**I)** Illustration of decreased expression of proliferation related genes in trabecular
846 CMs and ECM-associated genes in CECs of *Hdac3*^{tko} hearts.

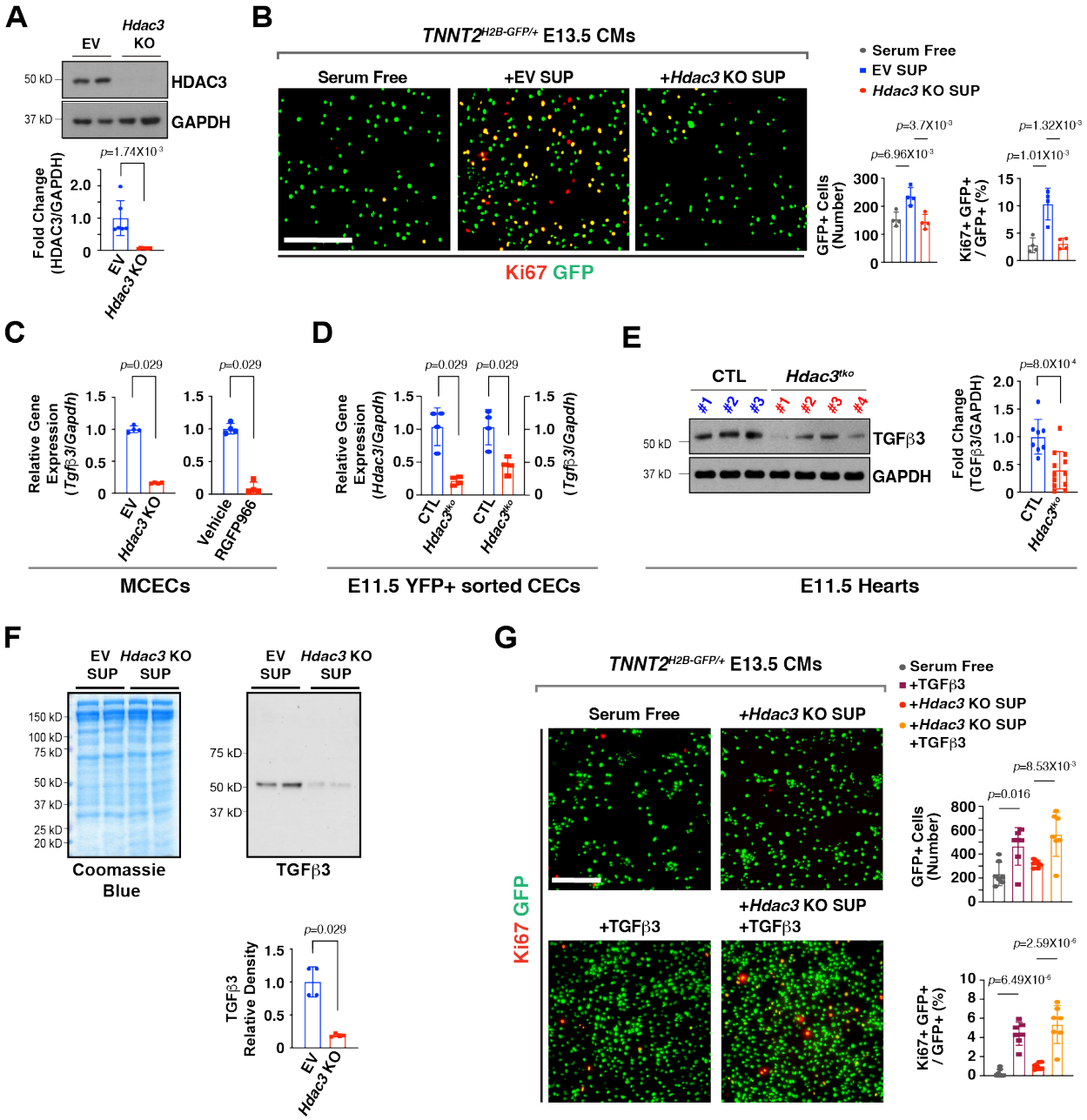

Figure 3. Cardiac endothelial *Hdac3* knockout results in downregulation of TGFβ3 and decreased cardiomyocyte proliferation.

(A) Generation of *Hdac3* knockout (KO) and empty vector control (EV) mouse cardiac endothelial cells (MCECs) by CRISPR/Cas9. Deletion of *Hdac3* was verified by western blot. Quantification is shown below (n=6 in each group). **(B)** The effects of *Hdac3* KO

853 MCEC supernatants on E13.5 *Tnnt2*$^{nGFP/+}$ cardiomyocytes (CMs) proliferation.
854 Representative immunofluorescence micrographs are shown. Scale bar, 275 μm.
855 Percentage of Ki67+ CMs and total number of GFP+ CMs were quantitated (n=4 in each
856 group). **(C)** Quantification of *Tgfβ3* expression in *Hdac3* KO MCECs, or RGFP966-treated
857 MCECs (10 uM) by qRT-PCR. *Gapdh* was used as cDNA loading control (n=4 in each
858 group). **(D)** Downregulation of *Tgfβ3* gene expression in *Hdac3* deficient cardiac
859 endothelial cells. YFP+ E11.5 cardiac endothelial cells (CECs) from *Hdac3*^{tko} (*Hdac3*$^{f/f}$*;*
860 *Tie2-Cre/+; R26*$^{eYFP/+}$) and CTL (*Hdac3*$^{f/+}$*; Tie2-Cre/+; R26*$^{eYFP/+}$) hearts were sorted by
861 fluorescence-activated cell sorting. Quantification of *Hdac3* and *Tgfβ3* expression by
862 qPCR was shown on the right. n=4 for each group. *Gapdh* was used as cDNA loading
863 control (n=4 in each group). **(E)** Representative Western blot and quantification of TGFβ3
864 expression in E11.5 *Hdac3*^{tko} hearts (n=12) and littermate CTL hearts (n=8). **(F)** Secretion
865 of TGFβ3 from *Hdac3* KO and EV MCECs. Coomassie brilliant blue staining of total
866 extracted proteins from supernatants served as protein loading controls. TGFβ3 in the
867 MCEC supernatants were detected by western blot. Quantifications are shown on the
868 right (n=4 in each group). **(G)** Rescue of CM proliferation defect by *Hdac3* KO MCECs
869 supernatant supplemented with recombinant TGFβ3 (working concentration: 250 ng/ml).
870 Representative immunofluorescence micrographs are shown. Scale bar, 200 μm.
871 Percentage of Ki67+ CMs and total number of GFP+ CMs were quantitated (n=7 in each
872 group). *P*-values were determined by unpaired two tailed Student's *t*-test for **(A)** and **(E)**,
873 Mann-Whitney U test for **(C)**, **(D)** and **(F)** and one-way ANOVA followed by the Tukey
874 post hoc test for **(B) and (G)**.
875

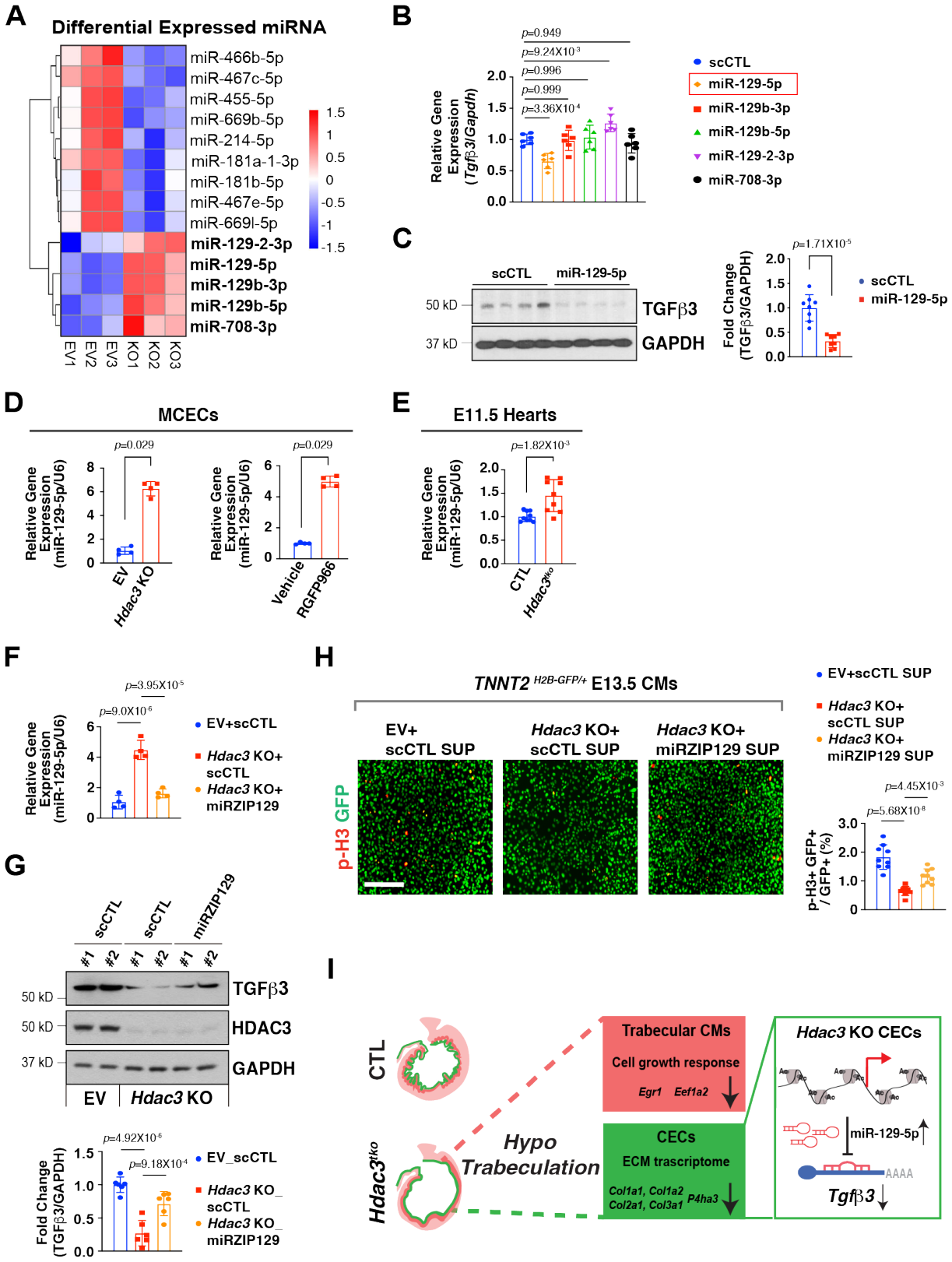
A
Differential Expressed miRNA
miR-466b-5p
miR-467c-5p
miR-455-5p
miR-669b-5p
miR-214-5p
miR-181a-1-3p
miR-181b-5p
miR-467e-5p
miR-669l-5p
miR-129-2-3p
miR-129-5p
miR-129b-3p
miR-129b-5p
miR-708-3p
EV1 EV2 EV3 KO1 KO2 KO3
B
Relative Gene Expression (Tgfβ3/Gapdh)
p=0.949
p=9.24X10-3
p=0.996
p=0.999
p=3.36X10-4
scCTL
miR-129-5p
miR-129b-3p
miR-129b-5p
miR-129-2-3p
miR-708-3p
C
scCTL
miR-129-5p
50 kD
37 kD
TGFβ3
GAPDH
Fold Change (TGFβ3/GAPDH)
p=1.71X10-5
D
MCECs
Relative Gene Expression (miR-129-5p/U6)
p=0.029
EV
Hdac3 KO
Vehicle
RGFP966
E
E11.5 Hearts
p=1.82X10-3
CTL
Hdac3tko
F
p=3.95X10-5
p=9.0X10-6
EV+scCTL
Hdac3 KO+ scCTL
Hdac3 KO+ miRZIP129
G
scCTL
miRZIP129
#1 #2
TGFβ3
HDAC3
GAPDH
EV
Hdac3 KO
p=4.92X10-6
p=9.18X10-4
EV_scCTL
Hdac3 KO_ scCTL
Hdac3 KO_ miRZIP129
H
TNNT2 H2B-GFP/+ E13.5 CMs
EV+ scCTL SUP
Hdac3 KO+ scCTL SUP
Hdac3 KO+ miRZIP129 SUP
p-H3 GFP
p=4.45X10-3
p=5.68X10-8
p-H3+ GFP+ / GFP+ (%)
I
CTL
Hdac3tko
Hypo Trabeculation
Trabecular CMs
Cell growth response
Egr1 Eef1a2
CECs
ECM trascriptome
Col1a1, Col1a2 Col2a1, Col3a1 P4ha3
Hdac3 KO CECs
miR-129-5p
AAAA
Tgfβ3

876

877 **Figure 4. HDAC3 induces Tgfβ3 by repressing miR-129-5p.**

878 **(A)** Heatmap of microRNA (miR) sequencing of *Hdac3* knockout (KO) and empty vector
879 control (EV) mouse cardiac endothelial cells (MCECs). MiRs with reads less than 100
880 were discarded and miRNA expression levels were normalized by TPM (transcript per
881 million) values (TPM = [miRNA total reads/total clean reads] × 10^6). Log_2 fold changes
882 were calculated by TPM per miR in the KO group divided by the mean TPM per miR in
883 the EV group then followed by calculation of Log (fold change, 2). Significantly
884 downregulated miRs are shown in blue, and significantly up-regulated miRs are shown in
885 red. Cut-off criteria: Log2>1.5 and adjusted *P*-value<0.01. **(B)** Quantification of the
886 expression of *Tgfβ3* in MCECs after miR mimics treatment (final concentration 10 nM) by
887 qRT-PCR. *Gapdh* was used as a cDNA loading control (n=6 in each group). Relative
888 gene expression was compared to the miR scrambles (scCTL) group. **(C)** Representative
889 Western blot and quantification of the expression of TGFβ3 after miR-129-5p mimics
890 treatment by western blot (n=8 in each group). **(D)** (Left) Quantification of *Tgfβ3*
891 expression in *Hdac3* KO and EV MCECs (n=4 in each group). (Right) Quantification of
892 the expression of *Tgfβ3* in MCECs after Hdac3 inhibitor treatment (RGFP966, final
893 concentration 5 uM) (n=4 in each group). **(E)** Quantification of the expression of *Tgfβ3* in
894 *Hdac3^{tko}* heart lysates (n=9 in each group). **(F)** Quantification of the expression of miR-
895 129-5p by qRT-PCR**.** *Hdac3* KO or EV MECs were transfected with LentimiRa-GFP-
896 miRZip129 (miRZIP129) or pGreenPuro Scramble Hairpin control lentivirus (scCTL) and
897 transfected cells were selected using puromycin (n=4 in each group)**. (G)** Representative
898 Western blot and quantification of the expression of TGFβ3 after treatment with
899 miRZIP129 or scCTL in *Hdac3* KO and EV MCECs (n=6 in each group). **(H)** Knockdown

900 of miR-129-5p rescues CM proliferation deficit induced by *Hdac3* KO MCEC supernatants.
901 Representative immunofluorescence micrographs are shown. Scale bar, 200 μm.
902 Quantification of percentage of phospho-histone H3 (p-H3)+ CMs was shown on the right.
903 Independent samples: n=9 in each group. The protein expression of TGFβ3 *P*-values
904 were determined by unpaired two tailed Student's *t*-test for **(C)** and **(E)**, the Mann-Whitney
905 U test for **(D)** and the one-way ANOVA followed by Tukey post hoc test for **(B)**, **(F)**, **(G)**
906 and **(H)**. **(I)** Working model: in the developing endocardium, HDAC3 represses the
907 expression of miR-129-5p to release their suppression on the expression of TGFβ3.
908 When *Hdac3* is deleted, the expression of miR-129-5p is increased, which subsequently
909 suppresses the expression of TGFβ3 to a stronger extent, and the decrease of TGFβ3,
910 together with decreased ECM, leads to hypotrabeculation.